Inorganic Materials, Vol. 36, No. 4, 2000, pp. 343–351. Translated from Neorganicheskie Materialy, Vol. 36, No. 4, 2000, pp. 431–439.

Effect of Precipitation Conditions on the Phase Composition, Particle Morphology, and Properties of Iron(III,II) Hydroxide Precipitates

A. G. Belous, E. V. Pashkova, V. A. Elshanskii, and V. P. Ivanitskii

Institute of General and Inorganic Chemistry, National Academy of Sciences of Ukraine, pr. akademika Palladina 32/34, Kiev, 252142 Ukraine

Received June 2, 1998; in final form, December 18, 1998

Abstract—The phase composition and particle shape of amorphous iron hydroxide–iron oxide precipitates were correlated with the oxidation state of iron in the starting solution, Fe_2O_3 : FeO ratio, and precipitation procedure (coprecipitation or successive precipitation) using Mössbauer spectroscopy, atomic absorption, low-temperature nitrogen BET, and electron microscopy data. A correlation was established between the amount of iron(II) in the starting solution, the amount of the metastable phase γ-Fe_2O_3 in the precipitate, particle shape, and the activity of the final heat-treatment products—α-Fe_2O_3 and mixed oxides of iron.

INTRODUCTION

In recent years, researchers engaged in the synthesis of ferromagnetic oxide materials have recognized the advantages offered by chemical homogenization of ferrite-forming components [1–4]: the assurance of high chemical uniformity and activity of the resulting ferrite powders [5]. Among chemical homogenization methods, hydroxide precipitation, a cheap and environment-friendly process, appears to be the most attractive. The properties of ferrites and their reproducibility depend strongly on the physicochemical properties of the starting reagents, particularly on those of the iron compound. All types of ferrites contain large proportions of an iron constituent, which forms their structural basis [5]. In view of this, it is always important to characterize the starting iron compound.

Earlier studies [6–12] were concerned with the preparation of iron oxide pigments and magnetic fillers for recording media, and their main purpose was to obtain certain modifications of iron hydroxides and oxides with particle-shape anisotropy.

In this work, we report the phase composition and particle morphology of iron hydroxide precipitates and the properties of their final heat-treatment product—α-Fe_2O_3 and mixed iron oxides—in relation to the oxidation state of iron in the starting compound, Fe_2O_3 : FeO ratio, and the way iron(III) and iron(II) hydroxides precipitate (coprecipitation or successive precipitation). These data were obtained by Mössbauer spectroscopy, atomic absorption, low-temperature nitrogen BET measurements, x-ray diffraction, and electron microscopy.

EXPERIMENTAL

Mössbauer spectra were recorded on an electrodynamic-type spectrometer operated at a constant acceleration (^{57}Co/Cr γ-source with an activity of 50 mCi; sample temperature, 300 or 77 K; source temperature, 300 K). Mössbauer data were processed by least squares.

Trace analysis was performed on a Unicam SP-9 atomic absorption spectrometer. In x-ray diffraction analysis, we used a DRON-3M diffractometer (FeK_α radiation). Particle morphology was studied by light microscopy (UEM-100K microscope) and scanning electron microscopy (JCXA-733 electron probe x-ray microanalyzer). Electrical and magnetic parameters were measured by standard procedures [13].

Hydroxides were precipitated from 2 M solutions of $Fe_2(SO_4)_3$, $FeSO_4$, or their mixture and concentrated NH_4OH at a fixed or variable pH, with the reactants simultaneously fed into the reactor. We varied the Fe_2O_3 : FeO ratio and used coprecipitation or successive precipitation. In the latter case, iron(II) hydroxide was precipitated onto iron(III) hydroxide precipitate. The products were aged for 15 h. We examined precipitates dried in a desiccator and those calcined subsequently at 1070 K.

RESULTS AND DISCUSSION

The hydroxide precipitates are known to suffer from low filtration coefficients and are therefore difficult to wash free of impurity ions. The properties of the precipitates were reported [14] to depend strongly on the precipitation pH and temperature. In view of this, we undertook the determination of the filtration coefficient

0020-1685/00/3604-0343$25.00

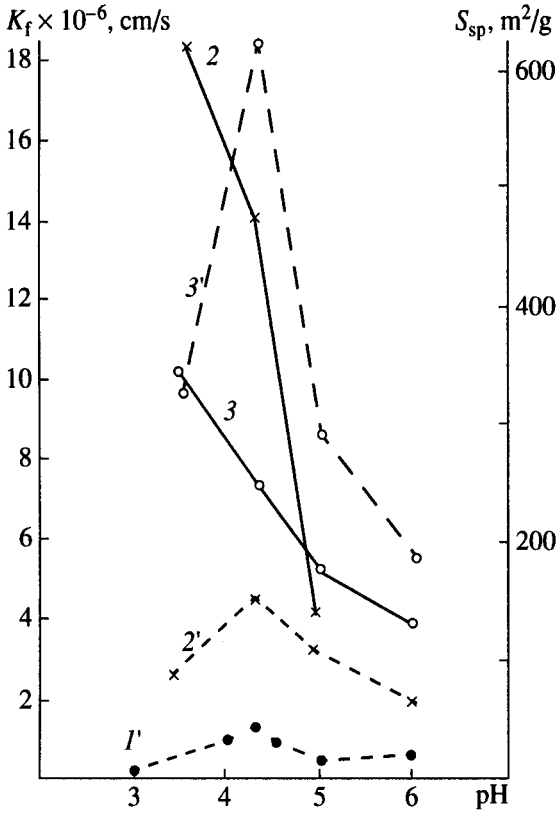

Fig. 1. (*2*, *3*) Specific surface area S_{sp} and (*1'*–*3'*) filtration coefficient of the precipitate as functions of precipitation conditions: (*1'*) variable pH, T = 288 K; (*2*, *2'*) fixed pH, T = 288 K; (*3*, *3'*) fixed pH, T = 320 K.

K_f and specific surface area S_{sp} of iron hydroxide as a function of these parameters. Iron hydroxide was prepared from a 2 M solution of iron(III) sulfate at (**I**) a constant pH and (**II**) a pH varied during the process to a specified value by continuously adding the precipitant.

The filtration coefficient of freshly prepared precipitates was determined as described in [15].

Our K_f and S_{sp} data are presented in Fig. 1. For both precipitation procedures and precipitation temperatures of 288 and 320 K, K_f peaks at pH 4.1 to 4.25 (pH was measured with an accuracy of ±0.1).

K_f in procedure **I** is 3–3.5 times larger than that in procedure **II** (Fig. 1, curves *1'*, *2'*). Raising the precipitation temperature from 288 to 320 K causes a two- to fourfold increase in K_f (curves *2'*, *3'*) and a marked decrease in the S_{sp} of the precipitate (curves *2*, *3*) and, therefore, its activity. After washing with equal amounts of water, the precipitates prepared by procedure **I** contained 1.7–2.0 times less foreign cations than the precipitates prepared by procedure **II**. Based on these results, we optimized the conditions for iron(III) hydroxide precipitation. Table 1 lists the conditions under which the precipitates were prepared.

The Mössbauer spectra of the as-precipitated samples 1–4 (Table 1) are presented in Fig. 2, and Mössbauer data for the precipitates and their heat-treatment products are listed in Table 2.

The spectrum of the sample prepared by precipitation from an $Fe_2(SO_4)_3$ solution (Fig. 2a, Table 2) consists of a single quadrupole doublet with parameters typical for the high-spin Fe^{3+} ion in octahedral oxygen coordination. Reducing the temperature from 300 to 77 K causes a marked broadening of the doublet components (Fig. 2b, Table 2), indicative of a relaxation process, presumably due to a small size of the superparamagnetic particles.

The spectrum of sample 2 consists of three sextets. The sextet with H_{eff} = 37440 kA/m and S = 4% was assigned to γ-Fe_2O_3, and the other two were assigned to goethite, α-FeOOH (Fig. 2c, Table 2).

The spectrum of sample 3 consists of four sextets (Fig. 2d, Table 2). Based on analysis of available data [16, 17], the two sextets with higher H_{eff} values and a total area of 67% were assigned to maghemite, γ-Fe_2O_3, and the other two were assigned to α-FeOOH [18, 19]. The separation of the second sextet for γ-Fe_2O_3 was made by mathematical means for a better resolution of the broad lines. Goethite is characterized by two sextets because its structure contains a considerable amount of water. As reported in [20, 21], when goethite contains 9–10 mol % water, its resonance lines are split into sextets with different H_{eff} values. According to Gendler *et al.* [20], the presence of water molecules in the goethite structure results in four possible nearest neighbor environments of the iron ion, realized with different probabilities, each giving its own Mössbauer signal.

The spectrum of sample 4, which differs in Fe^{2+} content from sample 2, consists of four sextets. The sextet with the greatest H_{eff}, 39280 kA/m, cannot be assigned with certainty to hematite, α-Fe_2O_3, which is characterized by H_{eff} = 41200–43200 kA/m. The 77-K spectrum of sample 4 clearly shows a sextet at H_{eff} = 43200 kA/m, assignable to α-Fe_2O_3. Relying on this assignment, the sextets with the greatest H_{eff} in the room-temperature spectra were attributed to a mixture of γ-Fe_2O_3 and α-Fe_2O_3 (Fig. 2e, Table 2).

As evident from the above data, the precipitates prepared from a mixture of ferric and ferrous sulfates contain γ-Fe_2O_3, whose proportion increases with Fe^{2+} concentration.

Figure 3 shows the Mössbauer spectra of as-precipitated samples 6–8 (Table 1), which were obtained from the $FeSO_4$ solution under different conditions, and that of sample 9, which was calcined at 1070 K. The parameters of the spectra are listed in Table 3.

The room-temperature spectra of these samples show closely spaced signals, which are characterized not only by a well-resolved doublet but also by a partially unresolved magnetic structure. The latter is evidenced by a "sag" in the spectrum and by the presence

of broad weak lines between the strong lines due to magnetically ordered phases. Computer deconvolution of the spectra, without regard for the unresolved magnetic structure, revealed two sextets with the following parameters: H_{eff_1} = 39520–40320 kA/m, IS_1 = 0.62–0.63 mm/s, QS_1 = 0.00–0.01 mm/s, H_{eff_2} = 37040–38800 kA/m, IS_2 = 0.06–0.62 mm/s, and QS_2 = –0.03 to +0.04 mm/s. These IS values suggest that the sextets, as well as the doublets, are due to the resonance absorption of γ-quanta by the nuclei of Fe^{3+} ions. The spectra taken at liquid-nitrogen temperature were characterized by higher H_{eff} values (H_{eff_1} = 42400–42800 kA/m, H_{eff_2} = 39520–40400 kA/m) and by the opposite sign of the quadrupole splitting. The observed H_{eff_1} values are characteristic of α-Fe_2O_3 only [22, 23]. The change of the sign of quadrupole splitting is explained by the Morin transition, which is observed in well-crystallized hematite [24]. The QS values of the first sextet at room temperature are somewhat lower than the reference values, which might be due to the presence of minute particles (which is evidenced by large halfwidths Γ and difficulties in spectrum deconvolution).

The parameters of the second, broader sextet allowed us to assign it to γ-Fe_2O_3.

As the sample temperature is decreased, the doublet due to Fe^{3+} in the spectrum of sample 6 disappears and that in the spectra of samples 7 and 8 weakens. This effect is explained by the superparamagnetism of minute particles of both α-Fe_2O_3 and γ-Fe_2O_3.

As seen from Fig. 3 and Table 3, a weak magnetic field applied to the precipitates obtained at pH 11 has no considerable effect on the α-Fe_2O_3 : γ-Fe_2O_3 ratio. However, at pH 9.5, an applied magnetic field raises the amount of γ-Fe_2O_3 from 64 to 76%.

Analysis of the signal from γ-Fe_2O_3 shows that, for the samples precipitated in a magnetic field, the second and fifth components are stronger than the first and sixth (Figs. 3c, 3d). This finding suggests that γ-Fe_2O_3 precipitated in a magnetic field has a collinear magnetic microstructure [25].

The dependence of the phase composition of the precipitate on the Fe^{2+} concentration in the starting solution, as derived from Mössbauer data (Tables 2, 3), is illustrated in Fig. 4. Analysis of this dependence provides insight into the mechanism of phase formation in mixtures of iron(III) and iron(II) hydroxides.

The observed correlation between the starting percentage of iron(II) and the percentage of the resulting γ-Fe_2O_3 (7% Fe^{2+}, 4% γ-Fe_2O_3; 31% Fe^{2+}, 32% γ-Fe_2O_3; 50% Fe^{2+}, 48% γ-Fe_2O_3) suggests that γ-Fe_2O_3 formation is confined to the volume of the forming

Table 1. Characteristics of precipitates

Sample no.	Starting reagents	Fe_2O_3 : FeO, weight ratio	Precipitation conditions
1	$Fe_2(SO_4)_3$	100 : 0	pH 4.25
2	$Fe_2(SO_4)_3$ + $FeSO_4$	93 : 7	Successive precipitation, pH 4.25, Fe(III)
			pH 9.5, Fe(II)
3	$Fe_2(SO_4)_3$ + $FeSO_4$	69 : 31	Coprecipitation, pH 9.5
4	$Fe_2(SO_4)_3$ + $FeSO_4$	69 : 31	Successive precipitation, pH 4.25, Fe(III)
			pH 9.5, Fe(II)
5	$Fe_2(SO_4)_3$ + $FeSO_4$	50 : 50	Successive precipitation, pH 4.25, Fe(III)
			pH 9.5, Fe(II)
6	$FeSO_4$	0 : 100	H = 0, pH 11.0
7	$FeSO_4$	0 : 100	H = 800 kA/m, pH 11.0
8	$FeSO_4$	0 : 100	H = 800 kA/m, pH 9.5

$Fe(OH)_2$ precipitate, as described by the following equations:

$$2Fe(OH)_2 + \frac{1}{2}O_2 \longrightarrow 2\alpha\text{-}FeOOH + H_2O, \quad (1)$$

$$Fe(OH)_2 + 2\alpha\text{-}FeOOH \longrightarrow Fe_3O_4 + 2H_2O, \quad (2)$$

$$2Fe_3O_4 + \frac{1}{2}O_2 \longrightarrow 3\gamma\text{-}Fe_2O_3. \quad (3)$$

Obviously, the α-Fe_2O_3 phase forms via goethite dehydration:

$$2\alpha\text{-}FeOOH \longrightarrow \alpha\text{-}Fe_2O_3 + H_2O. \quad (4)$$

Analysis of the correlation between the γ-Fe_2O_3 yield and the percentage of iron(II) in the starting solution for the two precipitation procedures (Table 2, samples 3, 4) clearly demonstrates that coprecipitation favors reaction between iron(III) and iron(II) hydroxides (coprecipitation: 31% Fe^{2+}, 70% γ-Fe_2O_3; successive precipitation: 31% Fe^{2+}, 32% γ-Fe_2O_3). These results are additional evidence of the occurrence of reactions (2) and (3).

Figure 5 shows the micrographs of precipitates 1, 3, 5, and 6 (Table 1). The hydroxide precipitated from an $Fe_2(SO_4)_3$ solution consists of platelike particles

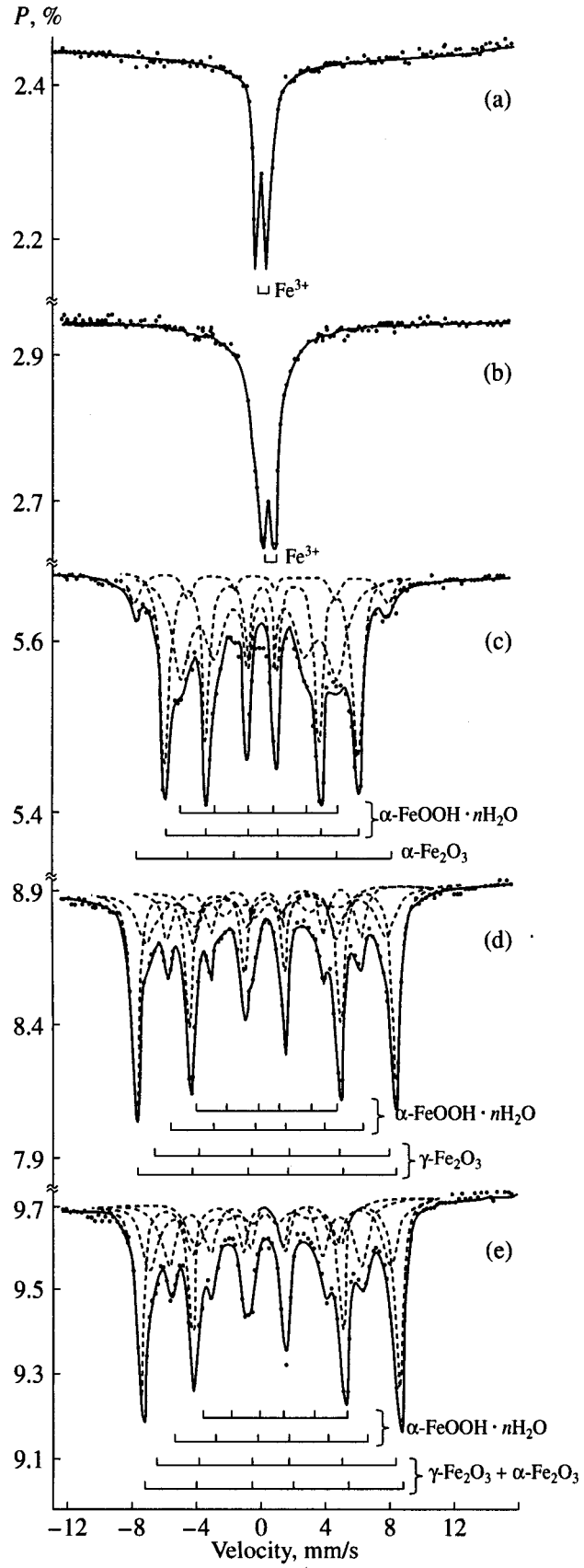

Fig. 2. Mössbauer spectra of as-precipitated iron(III,II) hydroxides for different precipitation procedures, oxidation states of iron in the starting solution, and Fe_2O_3 : FeO ratios: (a, b) sample 1, (c) sample 2, (d) sample 3, (e) sample 4. The spectra were recorded at (a, c–e) 300 and (b) 77 K.

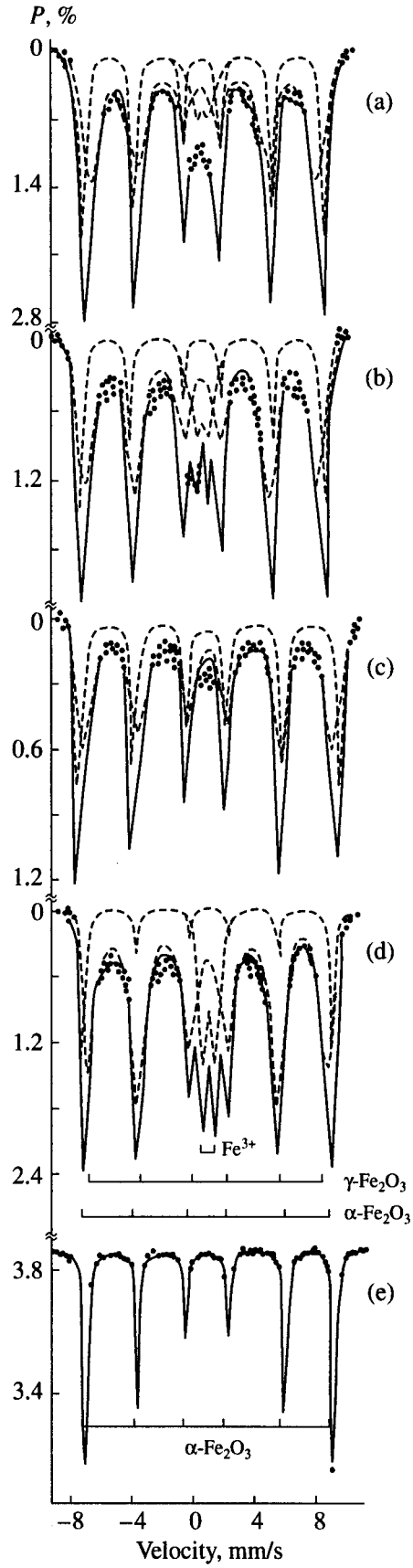

Fig. 3. Mössbauer spectra of iron(II) hydroxide samples prepared under different conditions: (a, b) sample 6, (c) sample 7, (d) sample 8, (e) sample 9. The spectra were recorded at (a, c, d) 300 and (b) 77 K. Sample 9 was calcined at 1070 K.

Table 2. Mössbauer data for iron hydroxides and oxides precipitated from iron(III) and iron(II) sulfate solutions

Sample no.	Phase composition		H_{eff}, kA/m	IS, mm/s**	QS, mm/s	Γ, mm/s	*S*, %
1(A)	Fe^{3+}		0	0.60(1)	0.72(2)	0.53(2)	100
1(A)*	Fe^{3+}		0	0.74(2)	0.80(2)	1.01(2)	100
1(B)	α-Fe_2O_3		41440	0.63(1)	0.22(1)	0.32(1)	100
2(A)	γ-Fe_2O_3		37440	0.65(4)	0.04(2)	0.60(1)	4(1)
	α-FeOOH	I	29760	0.66(2)	0.27(2)	0.58(2)	39(2)
		II	25280	0.67(2)	0.24(2)	1.8(1)	57(4)
2(B)	α-Fe_2O_3		41440	0.63(2)	0.22(1)	0.31(2)	100
3(A)	γ-Fe_2O_3	I	39520	0.60(2)	0.00(1)	0.58(2)	45(1)
		II	36080	0.68(2)	0.06(3)	1.30(5)	25(1)
	α-FeOOH	I	29280	0.66(2)	0.25(2)	0.63(3)	13(1)
		II	21840	0.71(2)	0.14(2)	0.89(3)	17(1)
3(B)	α-Fe_2O_3		41360	0.62(2)	0.23(2)	0.31(2)	100
4(A)	γ-Fe_2O_3		39280	0.58(2)	0.01(2)	0.53(1)	17(1)
	α-Fe_2O_3		38240	0.59(3)	−0.09(5)	1.00(6)	24(2)
	α-FeOOH	I	29360	0.59(2)	0.20(3)	1.00(5)	24(1)
		II	22000	0.74(9)	0.10(7)	0.98(7)	15(1)
4(A)*	γ-Fe_2O_3		42160	0.64(2)	−0.06(2)	0.58(1)	32(1)
	α-Fe_2O_3		43200	0.77(2)	0.07(2)	0.37(2)	20(1)
	α-FeOOH		40640	0.72(2)	0.23(2)	0.57(1)	48(1)
4(B)	α-Fe_2O_3		41440	0.63(2)	0.21(2)	0.32(1)	100
5(A)	γ-Fe_2O_3		39200	0.60(2)	0.01(2)	0.53(1)	48(2)
	α-Fe_2O_3		38240	0.60(3)	−0.10(5)	1.00(6)	19(1)
	α-FeOOH	I	29360	0.58(2)	0.20(3)	1.00(4)	17(1)
		II	22080	0.72(9)	0.10(7)	0.98(7)	15(2)
5(B)	α-Fe_2O_3		41440	0.63(2)	0.22(1)	0.31(2)	100

Notes: A and B label as-precipitated samples and samples calcined at 1070 K; QS = quadrupole splitting, Γ = line halfwidth, and *S* = site occupancy.

* Measurements were performed at liquid-nitrogen temperature.

** Isomer shift relative to sodium nitroferricyanide.

(Fig. 5a). Precipitation from a mixture of $Fe_2(SO_4)_3$ and $FeSO_4$ solutions yields needle particles at $C_{Fe^{2+}} \geq$ 31 wt % in the case of coprecipitation and at $C_{Fe^{2+}} \geq$ 50 wt % in the case of successive precipitation (Figs. 5b, 5c).

The preparation of iron hydroxide and oxide powders with a desired particle shape (platelike, cubic, spherical, needlelike) involves a number of additional operations such as feeding an oxygen-containing or reducing gas and adding a modifier [6–12]. By contrast, we observed spontaneous variation of particle shape. By relating the phase composition of the precipitates (Fig. 4) to their particle shape (Fig. 5), we inferred that the presence of γ-Fe_2O_3 favors the formation of needle particles. When this phase is present in a sufficient amount, the precipitate particles are nearly monodisperse. Such particles form during the coprecipitation of iron(III) and iron(II) hydroxides in the ratio corresponding to the magnetite stoichiometry or during precipitation from an iron(II) solution (Figs. 5b, 5d) if the product contains ≥70 wt % γ-Fe_2O_3 (Table 2, Fig. 4). Taking into account the structure of γ-Fe_2O_3 (defect spinel structure with a cubic close packing of oxygen

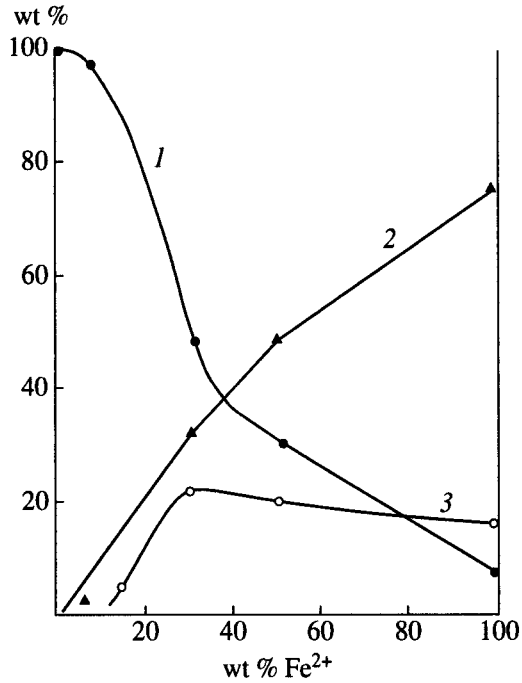

Fig. 4. Phase composition of as-precipitated iron hydroxide–iron oxide mixtures as a function of iron(II) concentration in the starting solution: (*1*) α-FeOOH, (*2*) γ-Fe_2O_3, (*3*) α-Fe_2O_3.

ions and tripled unit-cell parameter *a* along the fourfold axis, which coincides with the unique direction of easy magnetization [26]), one can infer that magnetic anisotropy favors particle-shape anisotropy. As seen from the micrographs, the needle particles of the samples prepared by coprecipitation of iron hydroxides in a ratio corresponding to the magnetite stoichiometry are aggregated into balls (Fig. 5b). This is apparently due to the predominantly electrostatic interaction between the particles under these conditions. Obviously, the shape of "secondary" particles, which result from heat treatment of precipitates, is determined by the orientation of the "primary" particles.

Calcining the precipitates at 1070 K yields single-phase α-Fe_2O_3 with unit-cell parameters characteristic of well-crystallized hematite. Although the starting amorphous powders differ in phase composition, the Mössbauer spectra of their heat-treatment products are identical and similar to the spectrum of α-Fe_2O_3 (Fig. 3e).

Table 4 lists the properties of α-Fe_2O_3 samples and magnesium–zinc ferrites prepared from them by standard ceramic processing.

Although α-Fe_2O_3 samples with different histories are structurally identical according to x-ray diffraction and Mössbauer data, they possess markedly different properties (Table 4). We explain this finding by the effect of the γ-Fe_2O_3 phase, present in the as-precipitated material, on the reactivity of the final product, α-Fe_2O_3. This explanation is supported by the fact that, as the proportion of γ-Fe_2O_3 increases, the rate of product dissolution in hydrochloric acid falls and its specific surface area and shrinkage ratio [27] grow (Tables 1, 4; Fig. 4). It is also supported by the properties of magne-

Table 3. Mössbauer data for iron hydroxide–iron oxide precipitates obtained from an iron(II) sulfate solution

Sample no.	Precipitation conditions	Phase composition	H_{eff}, kA/m	IS, mm/s	QS, mm/s	Γ, mm/s	*S*, %
6	pH 11	SP	0	0.69	0.90	1.03	8
	$H = 0$	α-Fe_2O_3	39520	0.63	0.00	0.46	33
		γ-Fe_2O_3	37040	0.61	0.03	1.28	59
6*	Same as above	α-Fe_2O_3	42400	0.72	0.02	0.48	36
		γ-Fe_2O_3	40160	0.73	0.06	1.16	64
7	pH 11	SP	0	0.62	0.90	0.97	11
	H = 800 kA/m	α-Fe_2O_3	40000	0.62	0.02	0.41	21
		γ-Fe_2O_3	38000	0.60	0.03	1.18	68
7*	Same as above	SP	0	0.68	0.67	0.31	3
		α-Fe_2O_3	42400	0.70	−0.04	0.50	33
		γ-Fe_2O_3	39520	0.72	0.04	1.37	64
8	pH 9.5	SP	0	0.64	0.72	0.51	11
	H = 800 kA/m	α-Fe_2O_3	40320	0.63	0.01	0.40	11
		γ-Fe_2O_3	38640	0.62	−0.03	1.17	78
8*	Same as above	SP	0	0.73	0.68	0.58	7
		α-Fe_2O_3	42800	0.73	−0.04	0.37	17
		γ-Fe_2O_3	40400	0.74	0.04	1.26	76

Notes: Measurement errors: H_{eff}, ±400 kA/m; IS, ±0.07 mm/s; QS, 0.07 mm/s; Γ, 0.07 mm/s; *S*, 10%. SP = superparamagnetic phase.
* Measurements were performed at liquid-nitrogen temperature.

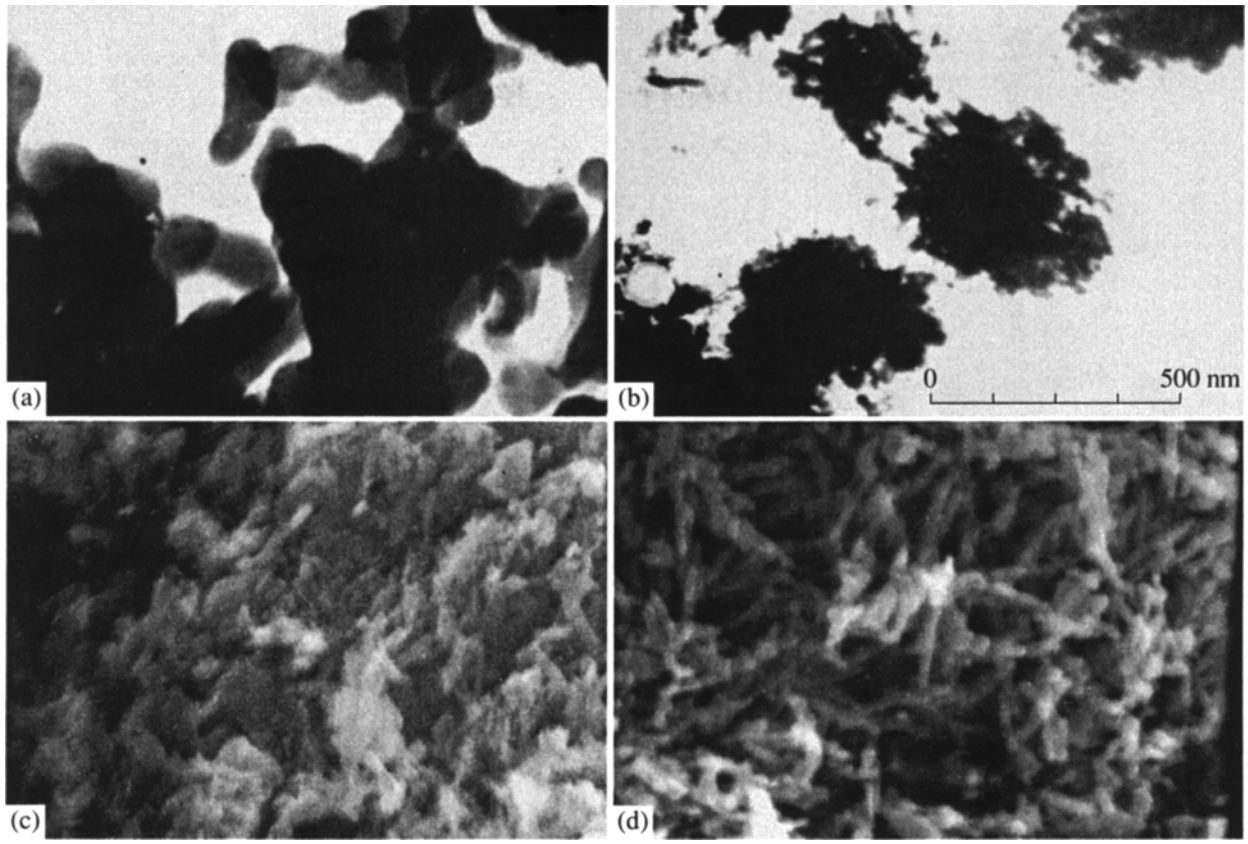

Fig. 5. Micrographs of precipitates (a) 1, (b) 3, (c) 5, and (d) 6 (Table 1); ×40000.

sium–zinc ferrites. The ferrites prepared from sample 1 (Table 1, Fig. 4) are characterized by low magnetic permeability and high magnetic losses. By contrast, samples 2 and 4, which were prepared from the precipitates containing 4 and 32 wt % γ-Fe_2O_3, respectively (Table 1, Fig. 4), ensure high quality of the ferrites. The effect of the large proportion of γ-Fe_2O_3 in the starting precipitate 3 is likely compensated for by the adverse effect of impurities, which are present in larger amounts because of the high coprecipitation pH.

Thus, the activity of α-Fe_2O_3 depends not only on whether or not it contains γ-Fe_2O_3, as noted in [5, 28], but also on whether or not the latter is present in the parent precipitate, even if it is absent in the oxide itself. Therefore, in the synthesis of α-Fe_2O_3 for ferromagnetic materials via hydroxide precipitation, it is essen-

Table 4. Properties of α-Fe_2O_3 and electrical and magnetic properties of manganese–zinc ferrites as functions of the conditions of α-Fe_2O_3 preparation

Sample no.	Properties of α-Fe_2O_3						Electrical and magnetic properties* of magnesium–zinc ferrite					
	wt % Fe_2O_3	total concentration of 17 impurities, %	S_{sp}, m^2/g	τ_{diss}, s**	K_{shr}, % (1270 K)	weight loss during calcination, %	H_c, A/m	μ_i	ρ, Ω cm	B_s, mT	P_v, mW/cm^3	
											295 K	350 K
1	99.4	0.19	4.8	151	10.2	0.41	22.3	1400	0.02	475	155	115
2	99.3	0.19	23.4	92	12.2	0.51	23.9	1950	0.93	480	105	65
3	99.1	0.36	11.5	102	13.7	0.54	24.7	1750	0.12	435	145	100
4	99.4	0.18	27.5	70	13.9	0.42	23.1	2000	0.19	445	115	75

* Coercivity (H_c), initial magnetic permeability (μ_i), saturation induction (B_s), and specific power loss (P_v) were measured at room temperature; B_s, at 800 A/m and 16 kHz; P_v, at 20 Pa and 16 kHz.

** Time of dissolution in 6 N HCl.

Table 5. Effect of the conditions of preparation of nickel–zinc ferrites on their properties (t_{sint} = 1240 K, τ_{sint} = 1 h)

Sample no.	Preparation conditions	S_{sp}, m^2/g**	d, g/cm^3	K_{shr}, %	ρ, Ω cm	σ_s, A m^2/kg
1	Coprecipitation	0.45	5.2	16.5	6.7×10^7	49.06
2	Successive precipitation on precipitate 1*	1.17	5.3	18.5	6.7×10^7	47.27
3	on precipitate 2	1.35	5.5	19.9	2.1×10^9	54.60

* For the characteristics of the precipitates, see Table 1.

** The specific surface area of the mixture for ferrite synthesis was determined from air permeability data for a compacted powder layer on a PSKh device [29].

tial to ensure γ-Fe_2O_3 formation in the hydroxide precipitate.

All the above is true for metal ferrite synthesis via hydroxide precipitation. Table 5 lists some properties of nickel–zinc ferrites whose compositions are similar to those of ZSCh-8 ferrites. The mixtures for ferrite synthesis were prepared by heat-treating coprecipitated iron(III), nickel, and zinc hydroxides (sample 1); nickel and zinc hydroxides precipitated on iron hydroxide (sample 2); and nickel and zinc hydroxides precipitated on the mixture of iron(III) and iron(II) hydroxides (sample 3). Even a small amount (4 wt %) of γ-Fe_2O_3, which was present in the parent precipitate of sample 3 (Table 1, Fig. 4), was sufficient to increase the activity (S_{sp}, K_{shr}, d) of the oxide mixture and to improve the electrical and magnetic properties (ρ, σ_s) of the sintered bodies.

Note that the coprecipitated hydroxides studied tend to form stable aggregates, and, therefore, they have a smaller specific surface area than do successively precipitated hydroxides (Tables 4, 5). The direct dependence of the activity of α-Fe_2O_3 and mixed oxides based on it on the presence of the metastable phase γ-Fe_2O_3 in the parent oxide–hydroxide precipitate (even when this phase is absent in the final product) testifies to a memory effect, which determines, to a great extent, the structure and properties of the ferrites [29].

CONCLUSION

The phase composition and particle shape of amorphous iron hydroxide–iron oxide precipitates are shown to depend on the initial oxidation state of iron, Fe_2O_3 : FeO ratio, and precipitation procedure (coprecipitation or successive precipitation).

A mechanism of phase formation in mixtures of iron(III) and iron(II) hydroxides is suggested.

There is a correlation between the amount of iron(II) in the starting solution, the amount of the metastable phase γ-Fe_2O_3 in the precipitate, particle shape of the precipitate, and the activity of the final heat-treatment product—α-Fe_2O_3 or mixed oxides of iron.

An applied magnetic field promotes γ-Fe_2O_3 formation in the precipitates and favors the collinearity of the magnetic structure.

The γ-Fe_2O_3 phase, when present in the precipitate in amounts of 70 wt % or more, favors the formation of monodisperse needle particles. At a lower γ-Fe_2O_3 content, the particles are platelike.

The results of the present study may be useful in optimizing the precipitation procedure and parent precipitate for ferrite synthesis.

ACKNOWLEDGMENTS

This work was supported by the National Science and Technology Committee of Ukraine, project no. 391.

REFERENCES

1. Chang, C.W., Tseng, M.S., and Wang, S.J., The Study of the Synthesis and the Magnetic Properties of *M*-type Strontium Hexaferrite from Chemical Coprecipitation, *J. Mater. Sci. Lett.*, 1990, vol. 9, no. 7, pp. 832–833.
2. Gruskova, A., Slama, J., Michalikova, M., *et al.*, Preparation of Substituted Barium Ferrite Powders, *J. Magn. Magn. Mater.*, 1991, vol. 101, nos. 1–3, pp. 227–229.
3. Jpn. Patent Application 3-14782, *Izobret. Stran Mira*, 1992, no. 37, p. 59.
4. Kioii Ogan, Jpn. Patent Application 2-28943, *Izobret. Stran Mira*, 1992, no. 37, p. 50.
5. Levin, B.E., Tret'yakov, Yu.D., and Letyuk, L.M., *Fiziko-khimicheskie osnovy polucheniya, svoistva i primenenie ferritov* (Physicochemical Principles of Preparation, Properties, and Applications of Ferrites), Moscow: Metallurgiya, 1979.
6. Kislitsyn, V.K., Nefedchenkov, V.M., and Rudenko, M.I., *Poluchenie poroshkov dlya nositelei magnitnoi zapisi* (Preparation of Powders for Magnetic Carriers), Leningrad: Khimiya, 1976.
7. Fefuchenkov, F.M., Pashaev, B.P., Rudenko, M.I., and Yakovlev, O.N., *Zhelezookisnye pigmenty* (Iron Oxide Pigments), Makhachkala: Dagestan. Knizhnoe Izd., 1974.
8. Bakare, P.P., Qupta, M.P., and Sinha, A.P.B., Mössbauer Spectroscopic Studies on Oxides and Hydrated Oxides

of Iron, *Indian J. Pure Appl. Phys.*, 1980, vol. 18, no. 7, pp. 473–478.

9. Ekkehard, S., Volker, A., Rainer, F., and Bernd, M., FRG Patent Application 3732526, *Izobret. Stran Mira,* 1989, no. 54, p. 30.
10. Jpn. Patent Application 2-34892, *Izobret. Stran Mira,* 1991, no. 37, p. 63.
11. Jpn. Patent Application 3-3612, *Izobret. Stran Mira,* 1991, no. 37, p. 56.
12. Jpn. Patent Application 2-220111, *Izobret. Stran Mira,* 1992, no. 37, p. 59.
13. *GOST* (State Standard) *12635-63: High-Frequency Soft-Magnetic Materials: Testing in the Range between 10 kHz and 1 MHz*, 1963.
14. Chalyi, V.P., *Gidrookisi metallov* (Metal Hydroxides), Kiev: Naukova Dumka, 1972.
15. Vaserman, I.M., *Khimicheskoe osazhdenie iz rastvorov* (Chemical Deposition from Solutions), Leningrad: Khimiya, 1980, p. 16.
16. Bauminger, R., Cohen, S.V., Marinov, A., *et al.*, Study of the Low-Temperature Transition in Magnetic and the Internal Fields Acting on Iron Nuclei in Some Spinel Ferrites Using Mössbauer Absorption, *Phys. Rev.*, 1961, vol. 122, no. 5, pp. 1447–1450.
17. Suzdalev, I.P., *Dinamicheskii effekt v gamma-rezonansnoi spektroskopii* (Dynamic Effect in Mössbauer Spectroscopy), Moscow: Atomizdat, 1979.
18. Nakamura, T. and Shimizu, S., Experimental Study on the Mössbauer Effect of Fe^{57} in Several Iron Compounds, *Bull. Inst. Chem. Res. Kyoto Univ.*, 1964, vol. 42, no. 5, pp. 299–318.
19. Takada, T., Kiyama, M., and Bando, J., Mössbauer Study of α-, β-, and γ-FeOOH, *J. Phys. Soc. Jpn.*, 1964, vol. 19, no. 9, pp. 1774–1779.
20. Gendler, T.S., Kuz'min, R.N., and Urazova, T.K., Mössbauer Study of Hydrogoethite, *Kristallografiya,* 1976, vol. 21, no. 4, pp. 774–781.
21. Hrynkilwiez, A., Kulgawezuk, D., and Tomala, K., Antiferromagnetism of α-FeOOH Investigated with the Mössbauer Effect, *Phys. Lett.*, 1965, vol. 17, no. 2, pp. 93–95.
22. *Chemical Applications of Mössbauer Spectroscopy*, Goldanskii, V.I. and Herber, R.H., Eds., New York: Academic, 1968. Translated under the title *Khimicheskoe primenenie messbauerovskoi spektroskopii*, Moscow: Mir, 1970.
23. Kyunding, V., Bemmel', G., Konstabadis, D., and Lindkvist, R.Kh., in *Issledovanie nekotorykh svoistv melkikh chastits* α-Fe_2O_3 *s pomoshch'yu effekta Messbauera* (Investigation of Fine-Particle α-Fe_2O_3 by Mössbauer Spectroscopy), Bugrov, I.A. and Sklyarevskii, V.V., Eds., Moscow: Atomizdat, 1969, pp. 222–238.
24. Fritzsch, E., Pietzsch, C., Heegn, H., and Huhn, H.J., The Morin Transition—A Sensitive Criterion for Testing the Quality of α-Fe_2O_3, *Cryst. Res. Technol.*, 1982, vol. 17, no. 11, pp. 1443–1447.
25. Bashkirov, Sh.Sh., Liberman, A.B., and Sinyavskii, V.M., *Magnitnaya mikrostruktura ferritov* (Magnetic Microstructure of Ferrites), Kazan: Kazan. Gos. Univ., 1978.
26. Tret'yakov, Yu.D., *Termodinamika ferritov* (Thermodynamics of Ferrites), Moscow: Khimiya, 1987.
27. Aron, P.M. and Palladieva, G.I., Methods for Assessing the Physicochemical Properties of Powder Ferrites, *Obz. Elektron. Tekh., Ser. Mater.*, 1976.
28. Rabkin, A.I., Soskin, S.A., and Epshtein, B.Sh., *Ferrity* (Ferrites), Moscow: Energiya, 1968.
29. Oleinikov, N.N., Ferrites: Evolution from Powder to Ceramic, *Zh. Vses. Khim. O–va. im. D. I. Mendeleeva,* 1991, vol. 36, no. 6, pp. 676–682.